Flexible, Air-Stable, High-Performance Heaters Based on Nanoscale-Thick Graphite Films

final version available at: https://doi.org/10.1021/acsami.1c23803

High-temperature, air-stable, flexible heaters based on nanorange graphite films

Geetanjali Deokar[1*], Abdeldjalil Reguig[1], Manoj Tripathi[2], Ulrich Buttner[1], Alberto Fina[3], Alan B. Dalton[2], Pedro M. F. J. Costa[1*]

[1] King Abdullah University of Science and Technology (KAUST), Physical Science and Engineering Division, Thuwal 23955-6900, Saudi Arabia
[2] Department of Physics and Astronomy, University of Sussex, Brighton BN1 9RH, United Kingdom
[3] Department of Applied Science and Technology, Polytechnic University of Turin, 15121 Alessandria, Italy

Abstract

Graphite sheets are known for their remarkable performance as heating panels and critical elements of thermal management systems. At an industrial scale, graphite films are fabricated using a high-temperature treatment of polymers or by calendering of graphite flakes, methods that limit their thickness to the micrometer scale. Here, we report a flexible and power-efficient cm^2 heater based on a semi-transparent polycrystalline nanorange graphite film (NGF, ~100 nm thick) grown by a CVD method. These NGF heaters operate stably over a wide range of temperatures (30-300ºC), demonstrated by their continuous heating at 215ºC and for 12 days in ambient conditions. With a fast ON/OFF switching response, the NGF can attain a steady peak temperature of 300°C, in air using a driving bias of 7.8 V (power density of 1.1 W/cm^2). The efficiency and flexibility of the NGF device are shown by externally heating a 2000 μm thick Pyrex glass vial and bring 5 ml of water to 96°C, in <20 min (with 2.4 W/cm^2). This performance is attributed to the peculiar characteristics of the NGF, which contains well-distributed wrinkles of variable size and micrometer-wide few-layer graphene domains. Taken together, the NGF stands to be an excellent choice of active material for ultra-thin, flexible heating panels that operate with a low-power source.

Keywords: Graphite film, Electrothermal heater, Low power, Flexible, Modeling

***Corresponding authors:** geetanjali.deokar@kaust.edu.sa; pedro.dacosta@kaust.edu.sa

Highlights

- Fabricated a cm^2 heating panel based on a nanorange graphite film (NGF, ~100 nm thick)
- Showed that a NGF/Kapton heater could be operated under a bent load
- Measured ON/OFF times to steady-state temperature (30-300°C) of a few seconds
- Demonstrated long-term operational stability in air (for 12 days) at high temperature (>200°C)
- Explained the enhanced heat transfer as a function of wrinkles and graphene domains in the NGF
- Assembled a NGF-based external heater to boil water inside a glass vial

Table of content figure

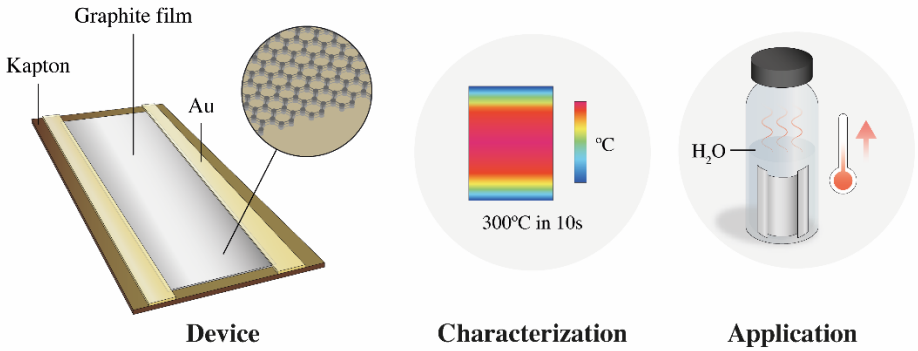

Low-power flexible heaters based on nanorange graphite films were fabricated and applied for heating water-filled glass vials

1. Introduction

Many of our daily home appliances (e.g., kettle, toaster) rely on resistive heating materials such as nickel-chromium alloys. Other less conspicuous technologies such as defogging devices in avionic/automobile windows and outdoor display panels [1, 2], microfluidic chips [3] and sensors [4-6] also require heaters. For these, more flexible and lightweight active materials are needed [7-10]. Classically, high-end heating devices have used ceramics and metals, the most common indium tin oxide (ITO) [11], fluorine tin oxide (FTO), poly-Si [5], and the moldable metal alloy Kanthal [2, 12]. Besides potential toxicity (e.g., chromium), limited precursor availability (e.g., indium), and/or complex manufacturing processes, these materials may not be appropriate for scaled-down devices due to brittleness, high mass density, or chemical reactivity [10, 13].

In recent years, the use of carbon nanomaterials in heating systems gained attention as this could lead to the manufacturing of low-power and flexi-transparent resistive panels. For instance, combining carbon nanotubes (CNT) and the electrically conductive polymer PSS: PEDOT enabled the fabrication of electronic-ink printed heaters with better performance than those based on ITO films [14, 15]. However, purification, bundle separation, and matrix dispersion are common process steps of CNT samples that, besides increasing manufacturing costs, may alter the electrical and thermal conductivities of these fillers [8, 10, 14, 16]. Furthermore, polymers and printing techniques inevitably limit this option to heating elements that are micro- to millimeter thick [8, 14, 16].

An alternative to CNTs, graphene has a low convective heat transfer coefficient, thereby enabling remarkable electrothermal device performances [17]. However, graphene-based heaters suffer from large sheet resistance, thus requiring a reasonably high input voltage (20 - 60 V) to attain their applicable operational temperature (50 - 250°C) [1, 18-20]. Several attempts have been made to overcome this issue: sequential transfer-and-stack of multiple graphene sheets, lattice doping, mixing with metallic nanoparticles or fabricating graphene-CNT hybrid structures [13, 17, 19, 21-23]. On the whole, these approaches add process steps that weigh against a lean and cost-effective workflow for future technology deployment. In addition to graphene sheets, resistive heating elements made from graphene-derivatives have been reported and include graphene oxide (GO) [21], reduced graphene oxide (rGO) [20], and laser-induced rGO (LrGO) [24, 25]. These have some advantages such as low production costs and simpler process workflows but suffer from batch-to-batch heterogeneity [25, 26] and relatively poor electrical conductivity [24, 25]. More importantly, graphene-derivative heaters are inherently limited regarding the maximum temperature of

operation [20, 25]. Upwards from 200°C, they start degrading in air [25] (due to a non-negligible concentration of structural defects), undergoing reactions that may be catalyzed if organic moieties or other elemental impurities are present [27].

Here we report a flexible and lightweight graphite film suitable for scaled-down heating devices. We show NGF-based heaters that operate at low input power (with voltages of <8 V reaching to 300°C) and have excellent stability in air. To demonstrate their remarkable efficiency, we used a NGF as the active material of an external adhesive panel to heat water in a glass vial.

2. Experimental Methods

Material growth and transfer

The NGF growth is described elsewhere [28]. Briefly, 25 μm Ni foils (purity: 99.5%, Goodfellow) were placed in a commercial chemical vapor deposition (CVD) reactor (BMPro 4", Aixtron GmbH), which was then purged with Ar and evacuated to 10^{-2} mbar. Next, the foils were heated to 900°C with a ramp rate of 75°C/min, in a mix of Ar/H_2 (500/1000 sccm), while maintaining a chamber pressure of 10 mbar. After this pre-annealing step (5 min dwell), the NGFs were deposited by exposing the Ni foils to a CH_4/H_2 flow (100 sccm each) and a chamber pressure of 500 mbar, at 900°C and for 5 min. The specimens were cooled down at a ~40°C/min rate, in an Ar flow (4000 sccm). Following their growth, a polymer-free wet-chemical transfer process (**Figures S1a - d**) placed the NGFs on target substrates. Details of the transfer process can be found in a previous report [29]. Note that deionized water (18 MΩ cm) was used during the transfer process. Hence, to improve the NGF's contact with the target substrates (in this work, Kapton, PET, quartz, or glass), the samples were placed in a vacuum furnace (10 mbar) and exposed to mild heat (70°C), overnight.

We have shown that the NGFs grow on both sides (front and back) of the catalytic Ni foils [29]. These carbon films have few-layer graphene (FLG, <10 layers) and multi-layer graphene (MLG, 10 to 30 layers) domains totaling 0.1% to 3.0% of their nominal area. The back-side film (BS)-NGF is relatively thinner (~80 nm) than the front-side (FS)-NGF one (~100 nm) and rougher (8 times higher root mean square roughness, as measured by AFM) [29]. We used NGFs from both sides for the fabrication of the heater devices.

Characterization techniques

Scanning electron microscopy (SEM) was performed with a FEI Nano Nova (1 - 5 kV, 50 pA). The structural analysis of the transferred NGFs (on Kapton) was carried out with powder X-ray diffraction, XRD (D8 Advance DaVinci, Bruker, with a Cu Kα source, λ = 1.5418 Å). The Raman spectroscopy analysis was done with a 532 nm laser (Alpha 300 RA, WITEC, 100 x Zeiss aperture, the optical probe of ~0.5 μm lateral resolution, and 25 mW of power). Conductive atomic force microscopy (C-AFM) used a Bruker Dimension Icon setup, placed inside an insulation box (to avoid external vibrations), and fitted with a PFTUNA tip (Bruker). The potential bias applied was 1 V (for all C-AFM measurements). The current-voltage (I-V) curves were acquired in a point-and-shoot ramp mode, in the bias range of -400 mV to 400 mV.

Heater fabrication and electrothermal response measurements

To fabricate the heaters, we used either the FS-NGF or the BS-NGF. Typically, the NGF was transferred from the Ni foil onto a Kapton sheet (25 μm or 125 μm thick - with maximum temperature stability of 400ºC, DuPont™) [30], following which the device was assembled (**Figures S1a - f**). Using a shadow mask, 200 nm thick Au electrodes were sputter-deposited (Quorum Q300TD) with a 2 mm overlap to the NGF sides. Crocodile clips were connected to the Au electrodes, using a Cu foil (30 μm) as a protecting interlayer (to avoid direct contact and damage to the Au thin film surface). For the application (water boiling), the NGF was transferred onto a 15 ml Pyrex glass vial (PGV) and connected to electrical wires with the assistance of a conductive Ag paste. To safeguard the wires during handling, a thin Kapton tape (25 μm) wrap was used.

The resistance of the NGF/Kapton samples was measured with a digital multimeter (Fluke 77 IV) at room temperature. To assess the electrothermal response, a voltage was applied from a direct current power supply (Agilent E3649A) to the Cu foil terminals of the NGF heaters held horizontally in the air, and thermal responses (to different driving voltages) were recorded. The local temperature readings and temperature distribution of the NGFs were measured by a focused infrared (IR) camera (Optotherm Micro, with a 20 μm resolution lens), placed right above the heating devices. Additionally, the water temperature inside the PGV was measured with a submerged digital thermometer. The temperature in the laboratory was controlled through a central air-conditioning system and varied between 22 – 25°C. Thus, with no applied voltage, the NGF/Kapton heaters were seen to fluctuate in the same range of temperatures.

Numerical modeling

The heat propagation, electrical and thermal properties of the NGFs [29] were studied using a finite element model that used the electrical and heat transfer modules integrated into the COMSOL Multiphysics software package [31, 32]. The computational work was carried out on a desktop workstation (3.7 GHz, 64 GB RAM, Supermicro SYS-5039A). To draw the heating device and model its components, we attended to the experimental size correlations and physical properties listed in public databases [31-35]. First, we designed a 4.5 cm^2 graphite film with uniform thickness (100 nm) and properties (i.e., a control sample for the active material). This carbon slab was placed on a 125 μm thick Kapton sheet. Next, the two Au electrodes (200 nm thick) were mounted on the left and right sides of the graphite and covered with a Cu film (30 μm thick). The surrounding environment was set as a block of air at 25°C. An electrical voltage was applied to one of its electrodes to operate the device model while the other was electrically grounded. The model for the NGF device was similar, differing only by the addition of an array of 100 few-layer graphene domains (shaped as 3 nm thick circles) in the graphite slab (**Figure S2**). To simplify the models, no wrinkles were included in the graphite and NGF slabs (this will be addressed in a follow-up modeling study). Also, the heat dissipation from the top surface of the graphite film to the surrounding air (through convection) was not considered as it is known to be negligible [32]. Finally, the calculated density-voltage (J-V) characteristics were validated with our experimental data and the work of Fang et al. [33].

3. Results

3.1. Morphological and structural analysis of NGFs

Recently, we reported the fast growth of NGFs on polycrystalline Ni foils [28]. These ~100 nm thick films have well-distributed wrinkles as well as domains of few-layer graphene (FLG, up to 3 nm of thickness) and multi-layer graphene (MLG, up to 10 nm), in a totaling areal density of 0.1% to 3.0% per 100 μm^2 [28, 29]. Here, the as-grown NGFs were first transferred to a flexible Kapton sheet by use of a polymer-free wet-chemical transfer process[29]., as illustrated in **Figure S1**. To demonstrate the flexibility of the NGFs, a typical NGF/Kapton sample was repeatedly bent and then characterized with SEM, Raman spectroscopy, and XRD (**Figures 1**, **S3,** and **S4**). As seen in **Figures 1a** and **S3**, the NGFs were intact (i.e., no cracks were identified). The structural quality of the mechanically stressed film was validated by Raman spectroscopy (**Figure 1b**). The

characteristic G (1583 cm^{-1}) and 2D (2658 cm^{-1}) peaks were observed (marked by blue arrows) and had an intensity ratio (I_{2D}/I_G ~0.3), correlating well with the typical values of a graphite film[29]. The absence of a D peak (commonly seen at ~1350 cm^{-1}) further indicates the crystallinity of the NGF was retained. The large area structural analysis, carried out by XRD, confirmed the NGF's integrity after repeated bending (**Figure S4** and respective description). This elasticity, allied to the high graphitization degree, is a desirable property for applying NGFs in miniature thickness electrothermal devices [21, 25, 36].

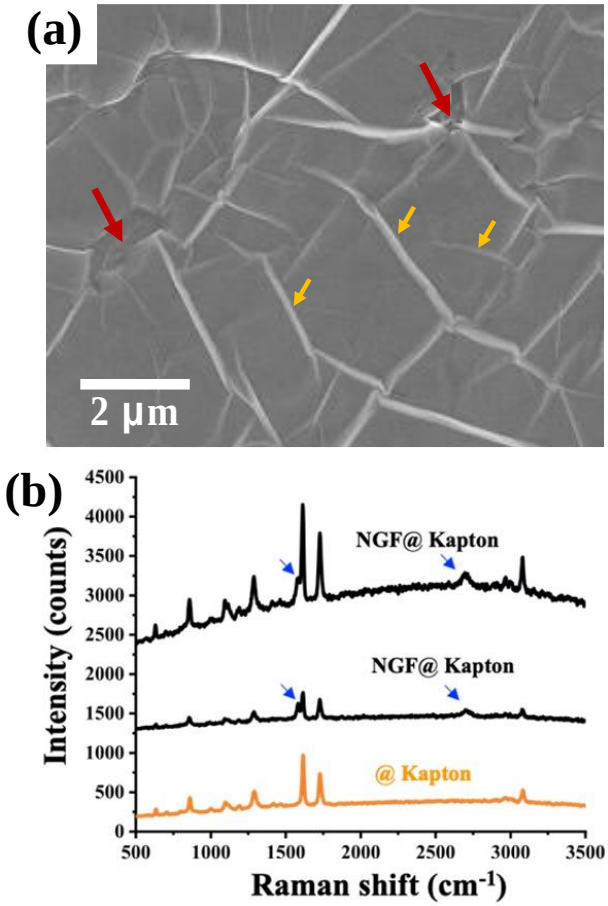

Figure 1. Surface morphology and structure of the NGF/Kapton: (a) SEM image showing the surface features of the graphite film where wrinkles of varied size (some marked with orange arrows) and FLG-MLG domains (red arrows) are observed. (b) Typical Raman spectra of the stack (NGF/Kapton) and the supporting polymer sheet (Kapton). The blue arrows point to the two fingerprint peaks of graphite (G and 2D).

3.2. Electrothermal performance

The electrothermal performance of the NGF/Kapton heaters (illustrated in **Figure 2a**) was studied in terms of ON/OFF switching response, applied bias and steady-state temperature. As

shown in **Figure 2b**, a typical heater device had an active NGF area of ~4.4 cm^2 and deposited Au electrodes which overlapped the sides of the NGF by ~(0.2 cm on each side). Unlike some thicker graphite heaters, our device retained the NGF flexibility and could be bent repeatedly (**Figure 2c**). Additionally, it had a significantly lower sheet resistance (10 - 50 Ω/sq, at room temperature **Figure S5** and reference [29]) than graphene (200 - 1,000 Ω/sq, **Table S1**).

To monitor the performance of the heaters, their temperature was measured as a function of time, when subjected to an electrical stimulus (DC voltage). In **Figure 2d**, a sharp temperature rise is observed that quickly stabilizes (in <10 s) at the system's steady-state temperature (for a fixed bias voltage). This plateau represents the maximum temperature (T_{max}) and remains constant as long as the bias is present (**Figure 2d**, for 120 s). Note that the bias was capped at 7.8 V, corresponding to an input of 4.9 W (over 4.4 cm^2), thereby establishing an upper limit for the T_{max} of 300ºC. Beyond this temperature, graphite films may start to oxidize in air (especially when considering the FLG domains present in the NGFs) [37, 38]. On switching off the power supply, the temperature drops rapidly. It reaches half of T_{max} within 10 s and room temperature (25ºC) in the following 30 to 90 s, depending upon the set T_{max} (**Figure 2d**). Other heaters based on carbon nanomaterials have also reported fast ON/OFF switching responses. For instance, Lin et al. demonstrated that a rGO film coated with Ag nanoparticles could reach 220ºC in only 5 s. [21] While considerably faster, their hybrid material needs three times higher operating voltage (18 V) to attain that temperature than our NGF (5.7 V). Otherwise, the response of our device is superior: (i) for a CNT/graphene hybrid heater, it takes 25 s to reach a T_{max} = 81ºC, at 12 V [19], (ii) for a rGO/g-C_3N_4 hybrid heater, it takes 60 s to reach a T_{max} = 78ºC, at 9 V [36].

In addition to the ON/OFF response, voltage and T_{max}, additional key factors in evaluating heating panels are i) the homogeneity of temperature distribution, ii) linearity of the thermal response, iii) input power density (W/cm^2, where W = current*voltage), and iv) structural durability.

i) Temperature distribution: on this point, the inset of **Figure 2d** is quite illustrative of the remarkably even spreads that the NGFs originate (with a T_{max} ~300ºC). The IR images were similar for all other cases investigated (with T_{max} = 27, 36, 150, and 212ºC, **Figure S6**). A more detailed inspection of the images revealed common trends in the temperature distribution. To illustrate these, we divided the active 4.4 cm^2 of the NGF into three regions, T_1 (or T_{max}), T_2, and T_3, as per the schematics in **Figure S6e**. For the example in the inset of **Figure 2d** (at 7.8 V), the T_{max}

(~300°C) occupancy corresponds to nearly 5% of the active area. Surrounding this, the T_2 is a region where the temperature drops to 93% T_{max} (~280°C), covering 90% of the area. As for the remaining 5% of the NGF, this corresponds to the T_3 region, heated at 60% T_{max} (~240°C). Obviously, the Au electrodes act as heat-sinks, explaining why the temperatures outside the active area remained close to room temperature (up to 30ºC). Taken together, the thermal profile is excellent and characteristic of a high-quality graphite film, with the central region accumulating the maximum energy (heat dissipation) due to the Joule heating effect [39]. It is worth noting that most heaters based on carbon nanomaterials [13, 17, 19-21, 25] or alternative materials [40], can only sustain a useful heating area of 60 to 100°C lower than ours.

ii) Linearity: the output linearity of the device was confirmed in the 1 V to 8 V interval (**Figure 2e**), with the T_{max} ranging from 30°C to 310°C, respectively. Of note, the minimum operating voltage of the heater was 0.5 V, denoting a high input sensitivity. Having observed an appropriate thermal distribution and the linear relation of temperature and applied bias, it is now possible to compare the NGF/Kapton power consumption with analogous systems in the literature.

iii) Power density: to contextualize the electrical current consumption of our heaters, the plot in **Figure 2f** provides the power density needed to attain T_{max} for several nanocarbon-based systems. The active materials range from graphene [13, 17], and CNTs [14, 19], to their hybrids [19], derivatives [20, 24, 36], and composites [10]. Note the data point labeled CNT-PEDOT: PSS-2021, reported by Pillai et al.[15]. Their device reached a T_{max} of 136ºC, at a power density of just 0.13 W/cm^2. While, in this parameter, the CNT composite is superior to our NGF/Kapton device (labeled NGF-2021 and with T_{max} ~90ºC, at 0.13 W/cm^2), their film is much thicker (13 µm), opaque (as opposed to the semitransparent NGF [29]) and has a maximum operational temperature limited by its matrix (the PEDOT: PSS melting point is ~146ºC).

iv) Durability: despite not being commonly discussed, the resilience of the active material to continued electrical stress, particularly when exposed to an oxidative atmosphere, is a key operational factor for resistive heating technologies. To investigate the structural durability of the NGFs, we selected an operating temperature well above the commonly reported for analogous nanocarbon-based heaters. As shown in **Figure 2g**, the device maintained a T_{max} of 215°C (5.71 V) for 12 days in air. The inset of **Figure 2g** shows the temperature map at the end of the durability test (for IR images recorded in other days, see **Figure S7** and **Video S1**). To the best of our knowledge, the NGF/Kapton assembly represents the lowest power consumption nanoscaled

carbon-based heater that is demonstrably operational for prolonged periods, in normal atmospheric conditions and the widest temperature range.

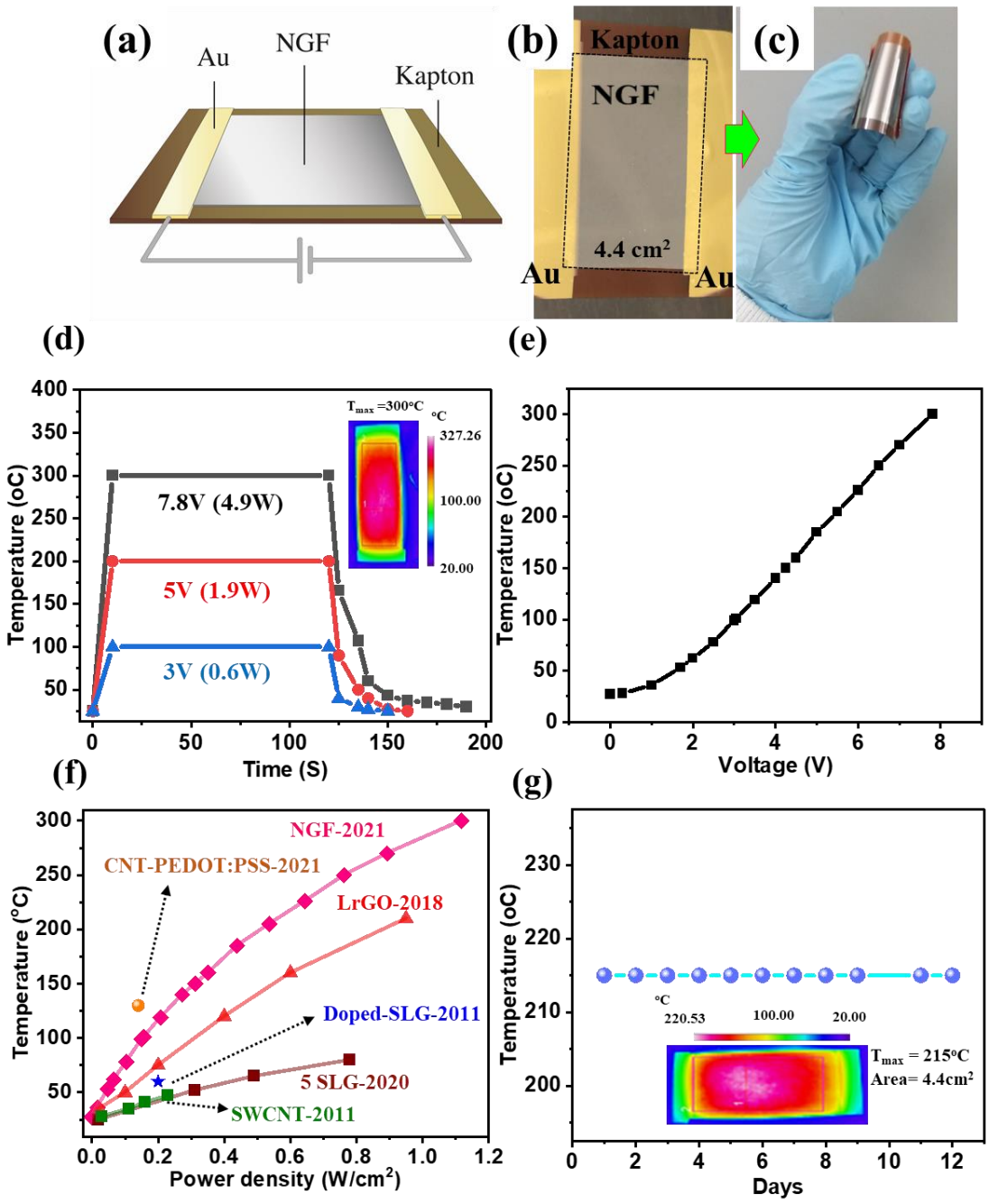

Figure 2. NGF/Kapton heater-electrothermal performance: (a) Schematic of the NGF heater set-up. (b,c) Digital images of a NGF/Kapton heater in its flat and bent configurations, respectively. (d) ON/OFF switching responses and steady-state temperatures (T_{max}) at three

different applied voltages; the inset shows a typical IR image taken for the heater at 7.8 V, when the T_{max} is 300°C. (e) The maximum temperature as a function of applied DC voltage, revealing a linear response at voltages higher than 1 V. (f) Comparative plot of the power density required to attain T_{max} for several nanocarbon-based heaters; besides the present NGF/Kapton (NGF-2021), the literature examples of active materials included are doped single-layer graphene (doped SLG-201)[13], few-layered graphene (5 SLG-2020)[41], laser reduced graphene oxide (LrGO-2018)[42], CNT-polymer composite (MWCNT-PEDOT-PSS-2021)[15], and single-walled CNT (SWCNT-2011)[43]. (g) Prolonged durability test (12 days) under normal atmosphere and an applied bias of 5.71 V; the inset shows the IR image taken at the end of the test, where T_{max} = 215°C.

NGF/Kapton as a flexible heater

As mentioned previously, the NGF/Kapton device could be bent, effortlessly and repeatedly, without breaking. In **Figure 3**, the operational capability of a flexed NGF heater is demonstrated. Added to its normal configuration (designated as a flat mode), two other cases were analyzed (bent modes 1 and 2, as illustrated in **Figure 3a**). Using a double-clamp mechanical system (home-build), the NGF device was carefully compressed, resulting in bending (**Figures 3b** and **3d**). Although it was not possible to measure the force applied, we regulated it by maintaining the Kapton sheet's curvature, with the two side-edges being at a distance of 1.8 cm (for the bent mode 1, this led to a curvature radius of 0.7 cm) or 1.5 cm (for mode 2, the radius of 1.1 cm). After several mechanical bending cycles, and irrespective of the mode considered, the electrothermal characteristics of the device were not altered (**Figure 3f**). This observation applies to the T_{max} just as well as to the temperature distribution and power consumption, as per the IR images of the bent NGF device subjected to a 7.8 V bias (**Figures 3c** and **3e**). Further, there was no measurable increase in sheet resistance or changes to the switching response times (**Videos S2** and **S3**). Taken together, these results validate the elasticity of the NGF/Kapton heaters and the potential to apply them not just in curved surfaces but also in flexible electronics.

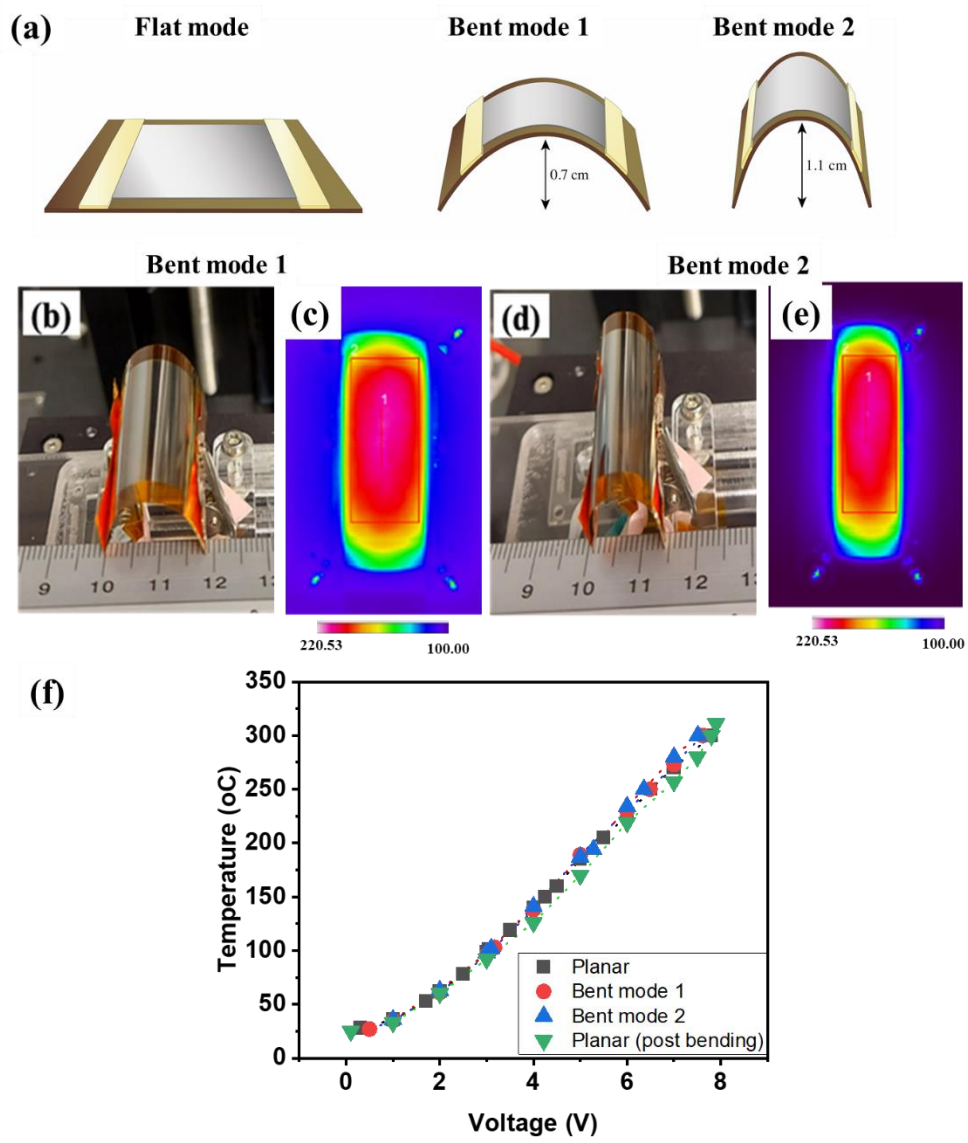

Figure 3. Operation of a NGF/Kapton heater subjected to a bending force: (a) Schematic of the flat and bent modes, including the Kapton's radius of curvature. (b) to (e) Digital photos of the setup in the bent modes 1 and 2, with respective IR images, taken at 7.8 V of applied bias; for both cases, the T_{max} = 300 °C and distribution is equal to that in the inset of Figure 2d. (f) Temperature versus voltage curves for the flat (pre- and post-bending) and bent modes; the linear response is maintained just as the minimum voltage required to activate the device (0.5 V).

Effect of wrinkles and few-layered graphene domains

The remarkable electrothermal performance of the NGF heaters prompted us to investigate its surface features and how these could contribute to the response of the active NGF. As previously shown (**Figure 1a**), the NGF surface consists of a network of wrinkles. Using AFM, we found their height ranged from 10 to 80 nm (**Figure 4a**). Then, to identify local variations in

the electrical conductivity of these corrugated surfaces, we employed C-AFM. Interestingly, the electrical map revealed a noticeable current drop on the wrinkles' positions compared to the continuous flat graphite regions. This is evident from the location of the darker areas in **Figure 4b** (marked with dashed lines), which correspond well with the surface protrusions identified in the topographic image (**Figure 4a**). Further, a more quantitative view of these differences is given by the I-V characteristics of the three main surface features studied: flat regions, small and large wrinkles. The flat regions (related to the basal planes of the graphite film and represented by the top-most black curve in **Figure 4c**) show an energy gap of 0.20 eV, as measured from the peak-to-peak distance in the first derivative I-V curve (dI/dV). This value is analogous to the non-zero bandgap of graphite films analyzed with other surface-sensitive techniques [44]. Considering the two wrinkles signaled in **Figure 4a**, with heights of 17 nm (small) and 70 nm (large), we observe that there is an enlargement of the electronic bandgap (0.36 eV and 0.60 eV, respectively) as the height of the wrinkles increases. This is consistent with the previous observation by Lu et al. of bandgap opening (0.23 eV) for strained graphene layers with the blister (height ~ 0.52 nm). It was reported that a local wrinkled configuration of graphene significantly affects the sheet resistance (increasing this resistance by up to one order of magnitude) and also reduces the mobility [45]. Accordingly, the arrays of wrinkles induce anisotropic transport properties, along with and across the folded configuration, through a mechanism of diffusive transport of charge [45] which favors the fast ON/OFF switching in contrast to a perfectly flat configuration of graphite sheet-based heaters. Thus, the band opening at the wrinkle's region and the localized anisotropy in charge transport could partially explain the enhanced thermoelectric properties of our NGF c devices.

Besides the wrinkles, one other surface feature that likely potentiated Joule heating was the junction between the ~100 nm film and its FLG domains. A finite element model (FEM) of the heating device, including the Kapton sheet, Au electrodes, and the NGF film, was developed to study this. Only the FLG domains and NGF-FLG interfaces were considered to simplify the model. Given the relatively small size of the FLG domains (inclusions on the order of micrometers in the cm-wide NGF), it was expected that these features would act as potential barriers and induce localized perturbations in the current flow, thereby slightly increasing the temperature in their surroundings (a.k.a. "hot-spots") [46]. In these circumstances, **Figures 4d** and **4e** show the temperature distribution found in two different models of the NGF/Kapton heater. The first shows a device with a regular graphite slab (100 nm thick) and acts as the control model (**Figure 4d**).

The second builds upon the control and includes the FLG domains and the corresponding NGF-FLG interfaces (**Figure 4e**). In both cases, the temperature gradient is expected, with the electrodes acting as heat-sinks and the central region of the graphite slab being the hottest point. However, for the same input of electrical power, the NGF clearly manifests higher temperature values. In fact, the simulated surface temperature shown in **Figure 4e** is in good agreement with the thermal map obtained experimentally (see IR image in **Figure S6d**). The absolute temperature values were extracted from the center to the edge of the modeled films (signaled with the dashed arrow Y_o in **Figures 4d** and **4e**). The respective profiles are presented in **Figure 4f**. In addition to a T_{max} difference of almost 50^{o}C, the presence of the FLG resulted in a wider T_{max} area. In practice, this means that the useful heating area at the target T_{max} (or close to it) is largely extended in relation to a normal graphite film. Such an observation correlates well with the 95% area that corresponds to the T_{max} and T_2 regions discussed above (**Figures 2** and **S6**). Also, note that a similar effect has been previously described for localized constrictions in graphene layers [47].

Taken together, the C-AFM and FEM studies help explain the superior performance of the NGF/Kapton devices. Briefly, in addition to the wrinkles (utterly common in CVD-grown graphene/graphite films), the FLG domains and NGF-FLG interfaces increase the diffusive charge transport characteristics of the active material, improving thereby the dissipation of energy as heat. This takes place without compromising the structural integrity of the NGF.

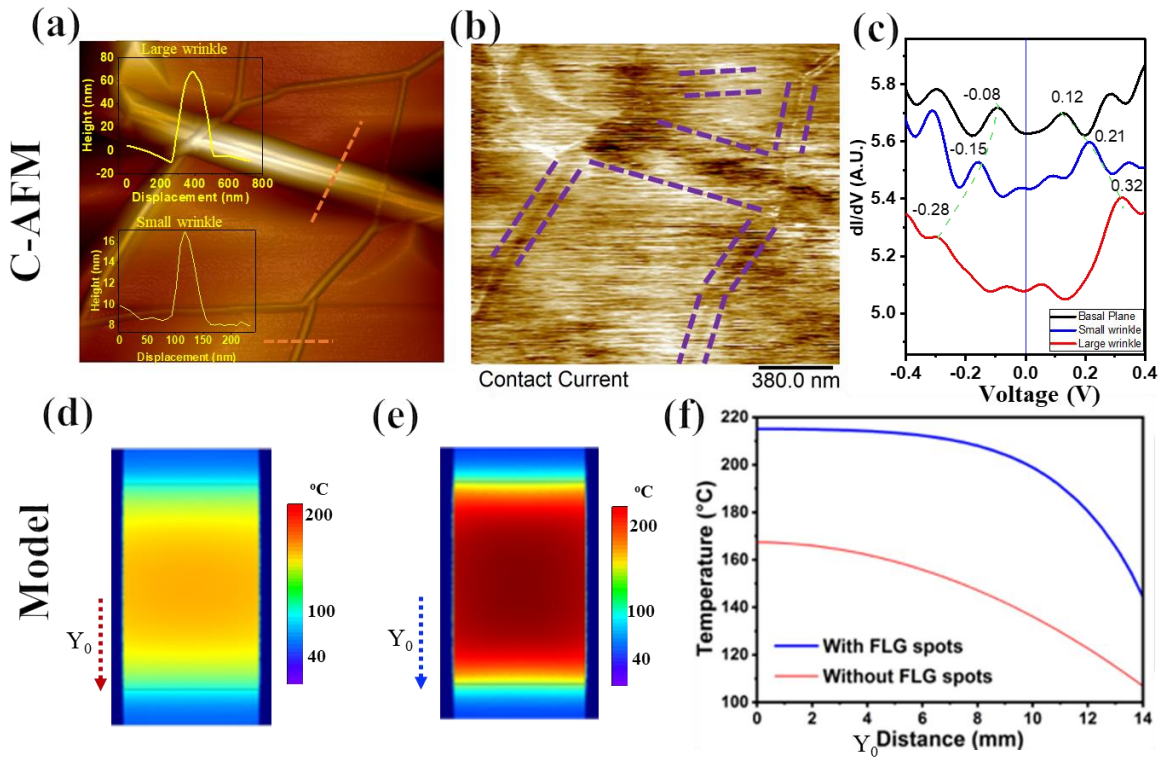

Figure 4. Analysis of the NGF surface features by C-AFM and FEM: (a) AFM topography image of the NGF surface; inset, height profiles of the two wrinkles crossed by the dashed lines and corresponding to a small (17 nm high) and large (70 nm) wrinkles. (b) C-AFM map of (a), showing the distribution of current (0.38 to 0.43 nA, at a bias voltage of 1 V) that spans typical flat regions and wrinkles; the lower current values are seen at the wrinkles, clearly identified by the darker contrast and delineated by the dashed lines. (c) The plot of the first derivative of current-voltage (dI/dV) versus voltage for the three surface features examined with C-AFM, basal plane (or flat region), small and large wrinkles; the dashed line highlights the increase of the bandgap with the height of the wrinkles and when to the flat regions. (d) FEM model of the control graphite/Kapton heater, when exposed to a bias of 5.7 V. (e) FEM model of the NGF/Kapton heater, where 100 FLG domains were distributed on the graphite surface, exposed to a bias of 5.7 V; the color scale of temperatures is equal to that in (d). (f) Temperature profiles were taken across the models in (d, red line) and (e, blue line), with their direction signaled by the dashed arrows (Y_0).

3.3. Application of the NGF device for water heating

The NGF's flexibility, durability, and high Tmax motivated us to assemble a water heating system to showcase its applicability. To do this, we transferred a BS-NGF directly (without Kapton) onto a 2000 μm thick wall of Pyrex glass vial (PGV). A conductive Ag paste fixed the BS-NGF to the PGV and the electrical cables of the power supply. This vial assembly (hereafter, labeled BS-NGF/PGV (2000 μm)) was integrated with a setup that included the IR camera. To

measure the water temperature, a partially submerged thermometer was used. The electrothermal response of the BS-NGF/PGV(2000 μm) could then be studied using two different configurations: (i) empty vials, as seen in **Figure 5a**, and (ii) filled vials, i.e., containing 5 ml of deionized water (**Figures 5b** and **S10**).

The following are the main findings of electrothermal response to the empty FS-NGF/PGV heater assembly:

- First, it was observed that rising the bias voltage led to a temperature increase not just on the NGF but also in its vicinity (outset of **Figure 5a** and **Figure S11**). Notwithstanding heat dissipation to the glass surface, the T_{max} - power density linearity was maintained, as seen in **Figure 5c** (data-curve labeled BS-NGF/PGV(2000 μm)). Note that the BS-NGF reached a T_{max} = 200°C when the input power density was 0.97 W/cm^2, which corresponds to an applied bias of 5.5 V. This voltage is slightly higher than the 5.0 V (0.54 W/cm^2) used for the FS-NGF device in **Figure 2f** (NGF-2021, re-labeled as FS-NGF/Kapton(125 μm) in **Figure 5c**). The variation is predominantly due to the substrate. The thermal mass of the thick glass (2000 μm) is significantly larger than that of the Kapton (125 μm). Additionally, the thermal conductivities of the Pyrex glass and the Kapton sheet are 1.1 W/m.K [48] and 0.12 W/m.K [30], respectively. Thus, a more pronounced heat loss would occur for the PGV set, resulting in a higher power requirement to attain the same T_{max}. This also explains the much slower ON/OFF response of the BS-NGF/PGV(2000 μm) assembly, which took almost two minutes to attain a steady-state T_{max} (compared with the few seconds of the FS-NGF/Kapton(125 μm), as shown earlier).

- Second, or the NGF/PGV assembly, we used Ag paste/electrical wires, as opposed to deposited Au electrodes/Cu sheet/crocodile clips of the earlier device, the sheet resistances (calculated from the I-V curves) differed only by 2/Sq, being slightly lower for the NGF/Au case. In fact, for our cm^2-scale heaters, we did not expect that electrode metal's choice would drastically affect their performance (in contrast to what happens in nanoscaled devices) [49].

- Third, the BS-NGF worked just as well as the FS-NGF though it drove a slightly higher power consumption. In addition to the BS-NGF/PGV(2000 μm), a device with a Kapton substrate was fabricated using the BS-NGF (labeled BS-NGF/Kapton(25 μm) in **Figure 5c**). Despite the reduced thickness of the polymer film, the electrothermal performance of this heater was poor than, for instance, the FS-NGF/Kapton(125 μm). Still, for a T_{max} = 200°C, the BS-NGF/Kapton(25 μm) required 0.79 W/cm^2, a lower value than the 0.88 W/cm^2 of the LrGO-2018 system (cf.

Figure 2f). Hence, for a high-temperature regime of (>150°C, in air), the NGFs are clearly superior to other reported nanocarbon-based heaters.

For the second configuration of the electrothermal response assessment, the BS-NGF/PGV(2000 μm) was filled with 5 ml of water, and the active material was positioned parallel to the line-of-sight of the IR camera (**Figure 5b**). In addition to this mounting ("vertical"- 90° with respect to the mounting surface, see also **Figure S9a**), two other NGF positions were probed. We named these "slightly inclined " - 50° with the mounting surface, (**Figure S9b**) and "inclined" - 20° with respect to the mounting surface (**Figure S9c**). During these experiments, the voltage was increased to 8.5 V, in steps of 1 V. At each bias increment, a dwell period of 2 min was maintained before recording the T_{max}.

In the "vertical" position, the water was at the same level as that of BS-NGF (placed on the outer side of the glass wall, **Figure 5b**). The corresponding electrothermal curve in **Figure 5c** is labeled BS-NGF/PGV(2000 μm). Upon reaching 8.5 V (2.37 W/cm^2), the T_{max} measured was 120°C, and the water temperature (T_{H2O}) was 96°C. Note that the IR image (taken at 8.5 V, outset of **Figure 5b**) captured only a fraction of the BS-NGF. As perceived from **Figure S10**, we could not displace the camera to capture the full extent of the NGF active area. Consequently, the T_{max} measured could effectively originate from the T_2 zone. Hence, the T_{max} is possibly underestimated by ~10% (refer to analysis in section 3.2). Nevertheless, it is clear that significant heat transfer through conduction mechanism occurs from the glass to the water, resulting in boiling of water (96°C) (see also **SI Videos 4a** to **4c**) when the NGF temperature is at 120°C.

For the other two orientations, the water level corresponded only partially to the area of the BS-NGF panel (Fi**gure S9b** and **c**). Logically, this translates into reduced conductive heat transfer/loss rates from the NGF to the water, justifying the inverse correlation of T_{max} (for equal input power density) versus inclination angle (**Figure S9**). Thus, for the "inclined" orientation, with a T_{max} = 260°C (8.0 V, 2.1 W/cm^2), the T_{H2O} did not surpass 40°C (**Figures S9c** and **S9f**).

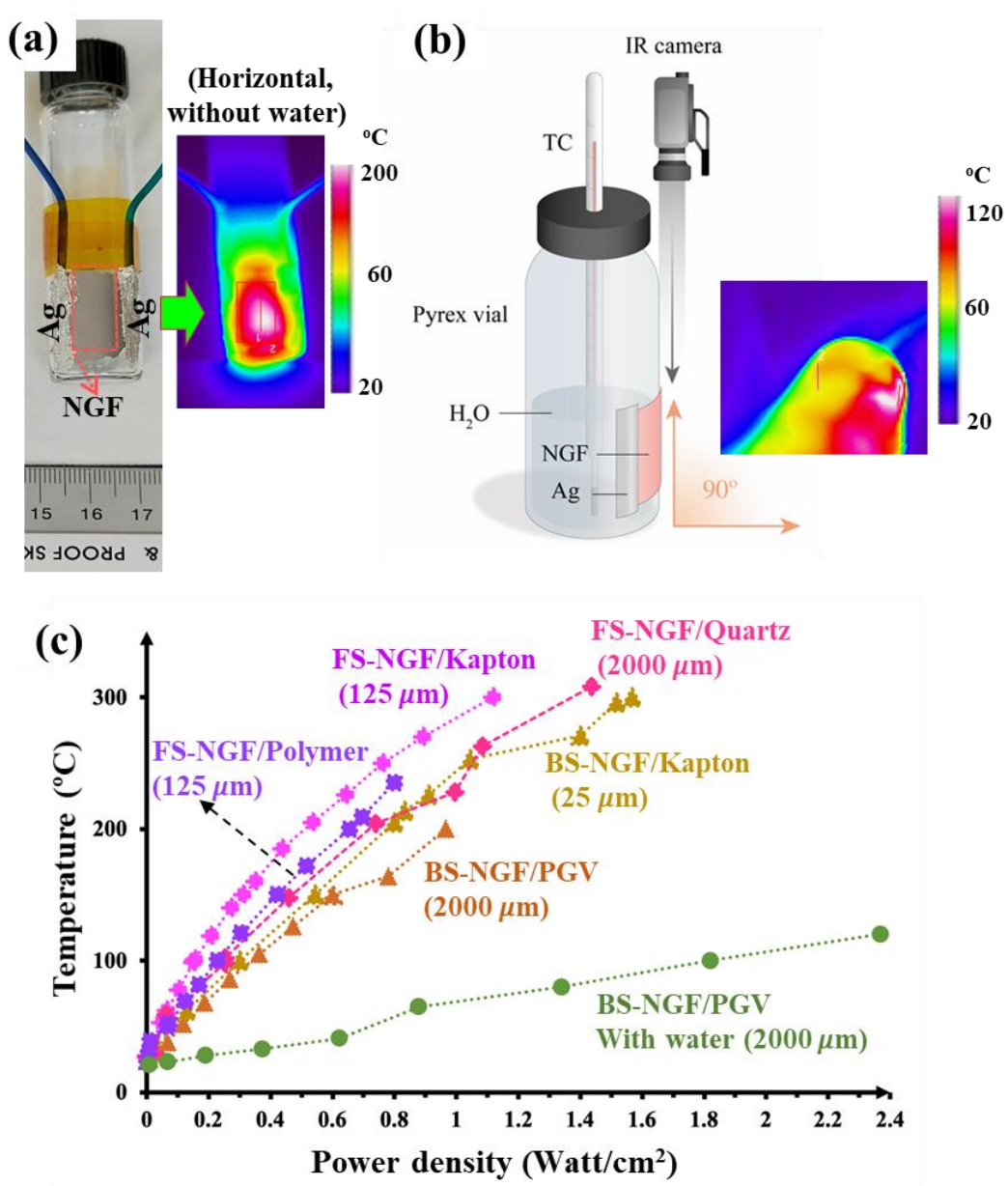

Figure 5. The use of NGFs for water heating and their electrothermal performance with different substrates: (a) Digital photo of the water heating device; this consisted in a BS-NGF placed on the outer wall of a glass vial and connected to two electrical wires via a conductive Ag paste; the outset shows the device's temperature map, at 5.5 V of applied bias. (b) Schematic of the device in (a), in an upright position and partially filled with water; also included is the digital thermometer for the water and the IR camera; the outset shows the device's temperature map, at 8.5 V of applied bias. (c) Electrothermal performance curves for different combinations of NGFs and substrates, including the PGV heater assembly; the labels are defined in the main text.

4. Discussion

The electrothermal study of NGF/Kapton heaters showed superior results in terms of low power requirement, response time, and maximum steady-state temperature when compared with other known carbon nanomaterials-based devices. Specifically, our heaters do not consume much voltage for the wide range of operational temperatures they operate in (from 30 to 300°C); they show an even spread of the target temperatures and have ON/OFF switch times on the scale of seconds. Furthermore, their mechanical flexibility and environmental stability are excellent.

In this study, the support Kapton sheet has high resistivity (1×10^{10} ohm-cm) [30], and it was assumed that no current leakage occurred through it. In fact, and regarding the substrates, we also considered a 25 μm Kapton, a 125 μm polyethylene-terephthalate (PET) sheet, and a 2000 μm quartz plate (all values refer to substrate thickness). As per the plot in **Figure 5c**, some interesting trends are apparent. First, the substrate type influences the power consumption, as the comparison between the 125 μm Kapton and 125 μm PET FS-NGF cases reveal. If a thick and insulating quartz plate (FS-NGF/Quartz(2000 μm)) is used, the power consumption will increase further. When compared to the other nanocarbons, it is remarkable that even the worst of our substrate options provides better consumption performance for temperatures above 150°C (**Figure 2f** and **Table S1** in supplementary information).

Following on the above, it is important to note that the sheet resistance of the NGF/Kapton heater was as low as 10 Ω/sq, this without having to undertake additional processing of the carbon film. The low sheet resistance and thermal capacity help understand our devices' performance. During Joule heating, the thermal power generated is directly proportional to the electrical power (P) provided, which is related to a driving voltage (V) and resistance (R) by $P = V^2/R$ or, equally, $P = R \cdot I^2$. We observed a rapid temperature rise of the entire film until it reached a saturation temperature within 10 s with applied voltage and a rapid drop to room temperature after voltage cut-off. This performance owes partly to the fact that the low sheet resistance of the NGF enables a high current for Joule heating. A fast ON/OFF response and good heat distribution of the generated heat over the cm^2-scaled area reflect the low thermal capacity of the film. In our case, a Kapton-supported NGF film demonstrated a steady-state temperature of 300°C at a low power density (applied voltage of 7.8 V), which outperforms previous reports (**Figure 2**, **Table S1**). Attainment of superior steady-state temperature, with a low applied voltage, reveals the outstanding performance of the heater by transduction of electrical energy into joule heating [22]. These heaters have excellent homogeneity of temperature distribution, explained by the presence

of a well-distributed few-layer domains and wrinkles on the NGF film [28, 29]. These surface features act as resistive hot spots as they are localized higher electrical resistance regions in the film, as confirmed by C-AFM measurements and the FEM study.

Considering recent trends and owing to the adaptability and conformability of the NGF heaters, our devices could find immediate application in the bio- or gas-sensing fields where samples need to be heated in the range of 30 - 300ºC [3, 5, 50-52]. In fact, removing atmospheric moisture is one of the critical challenges in graphene electronics. Generally, graphene heating (to ~100°C) is performed using bulky commercial heaters, requiring high power and occupying significant space [23]. In this respect, the NGF-based heaters could be easily implemented with a small footprint in the device [53, 54].

Conclusion

We developed a high-performance, cm^2-scaled flexible NGF-based heater with excellent environmental stability. To fabricate the NGF-based heaters, unlike graphene or other carbon materials heaters, a robust and straightforward one-step transfer onto the target substrate was performed without the need of multiple transfers, doping, functionalization, and/or nanoparticles loading. Excellent heat propagation in the air (up to 300ºC) and uniform temperature distribution, with fast switch ON/OFF responses was observed. Additionally, high-temperature stability was continuously monitored for up to 12 days. The nanoscopic imaging and modeling illustrated the presence of wrinkles and few-layer regions acting as a localized region of higher resistance (hot spots) and thus raising the overall heater temperature. Moreover, the remarkable performance of the flexible NGF heaters is demonstrated by boiling water in a Pyrex glass vial by a conductive heat transfer from NGF through a Pyrex glass to water. The availability of such flexible and low power coefficients of heating devices opens a window of opportunities that range from localized heating of laboratory-scale research samples to large-scale deployment as required in defoggers for aircraft and automobiles.

Author Contributions

GD: Conceptualization, experiments, analysis, original draft preparation, editing, and review. **AJ:** Modelling part editing and review. **UB:** Devise fabrication, editing, and inspection. **MT:** C-AFM

measurements, editing, and review, **AF:** editing and review, **AD**: resources, editing and review **PC:** Methodology, supervision, resources, editing and review

Acknowledgments

This work was supported by KAUST (BAS/1/1346-01-01). The KAUST Core Labs teams are acknowledged for the technical support. Alberto Fina acknowledges Mr. Fausto Franchini at Politecnico di Torino for helpful discussion. M.T. and A.B.D. are supported by the University of Sussex strategic development fund.

References

1. Mustonen, P.; Mackenzie, D. M. A.; Lipsanen, H., Review of fabrication methods of large-area transparent graphene electrodes for industry. *Frontiers of Optoelectronics* **2020,** *13* (2), 91-113.
2. Papanastasiou, D. T.; Schultheiss, A.; Munoz-Rojas, D.; Celle, C.; Carella, A.; Simonato, J. P.; Bellet, D., Transparent Heaters: A Review. *Advanced Functional Materials* **2020,** *30* (21).
3. Ortiz-Gomez, I.; Toral-Lopez, V.; Romero, F. J.; De Orbe-Pay, I.; Garcia, A.; Rodriguez, N.; Capitan-Vallvey, L. F.; Morales, D. P.; Salinas-Castillo, A., In situ synthesis of fluorescent silicon nanodots for determination of total carbohydrates in a paper microfluidic device combined with laser prepared graphene heater. *Sensor Actuat B-Chem* **2021,** *332*.
4. Kunti, G.; Dhar, J.; Bhattacharya, A.; Chakraborty, S., Joule heating-induced particle manipulation on a microfluidic chip. *Biomicrofluidics* **2019,** *13* (1).
5. Hwang, W. J.; Shin, K. S.; Roh, J. H.; Lee, D. S.; Choa, S. H., Development of micro-heaters with optimized temperature compensation design for gas sensors. *Sensors (Basel)* **2011,** *11* (3), 2580-91.
6. Chen, Z. C.; Chang, T. L.; Su, K. W.; Lee, H. S.; Wang, J. C., Application of self-healing graphene reinforced polyvinyl alcohol nanowires to high-sensitivity humidity detection. *Sensor Actuat B-Chem* **2021,** *327*.
7. Vertuccio, L.; De Santis, F.; Pantani, R.; Lafdi, K.; Guadagno, L., Effective de-icing skin using graphene-based flexible heater. *Compos Part B-Eng* **2019,** *162*, 600-610.
8. Janas, D.; Koziol, K. K., A review of production methods of carbon nanotube and graphene thin films for electrothermal applications. *Nanoscale* **2014,** *6* (6), 3037-3045.
9. Bhattacharyya, P., Technological Journey Towards Reliable Microheater Development for MEMS Gas Sensors: A Review. *Ieee T Device Mat Re* **2014,** *14* (2), 589-599.
10. Raji, A. R. O.; Varadhachary, T.; Nan, K. W.; Wang, T.; Lin, J.; Ji, Y. S.; Genorio, B.; Zhu, Y.; Kittrell, C.; Tour, J. M., Composites of Graphene Nanoribbon Stacks and Epoxy for Joule Heating and Deicing of Surfaces. *Acs Appl Mater Inter* **2016,** *8* (5), 3551-3556.
11. Kato, K.; Kuwahara, M.; Kawashima, H.; Tsuruoka, T.; Tsuda, H., Current-driven phase-change optical gate switch using indium-tin-oxide heater. *Applied Physics Express* **2017,** *10* (7).
12. Nguyen, B. H.; Nguyen, V. H., Promising applications of graphene and graphene-based nanostructures. *Adv Nat Sci-Nanosci* **2016,** *7* (2).

13. Kang, J.; Kim, H.; Kim, K. S.; Lee, S. K.; Bae, S.; Ahn, J. H.; Kim, Y. J.; Choi, J. B.; Hong, B. H., High-Performance Graphene-Based Transparent Flexible Heaters. *Nano Letters* **2011,** *11* (12), 5154-5158.
14. Yao, X. D.; Hawkins, S. C.; Falzon, B. G., An advanced anti-icing/de-icing system utilizing highly aligned carbon nanotube webs. *Carbon* **2018,** *136*, 130-138.
15. Pillai, A. S.; Chandran, A.; Peethambharan, S. K., MWCNT Ink with PEDOT:PSS as a multifunctional additive for energy efficient flexible heating applications. *Appl Mater Today* **2021,** *23*, 100987.
16. Yao, X. D.; Falzon, B. G.; Hawkins, S. C., Orthotropic electro-thermal behaviour of highly-aligned carbon nanotube web based composites. *Compos Sci Technol* **2019,** *170*, 157-164.
17. Bae, J. J.; Lim, S. C.; Han, G. H.; Jo, Y. W.; Doung, D. L.; Kim, E. S.; Chae, S. J.; Huy, T. Q.; Luan, N. V.; Lee, Y. H., Heat Dissipation of Transparent Graphene Defoggers. *Advanced Functional Materials* **2012,** *22* (22), 4819-4826.
18. Smovzh, D. V.; Kostogrud, I. A.; Boyko, E. V.; Matochkin, P. E.; Pilnik, A. A., Joule heater based on single-layer graphene. *Nanotechnology* **2020,** *31* (33).
19. Li, L. H.; Hong, S. K.; Jo, Y.; Tian, M.; Woo, C. Y.; Kim, S. H.; Kim, J. M.; Lee, H. W., Transparent, Flexible Heater Based on Hybrid 2D Platform of Graphene and Dry-Spun Carbon Nanotubes. *Acs Appl Mater Inter* **2019,** *11* (17), 16223-16232.
20. Sui, D.; Huang, Y.; Huang, L.; Liang, J.; Ma, Y.; Chen, Y., Flexible and transparent electrothermal film heaters based on graphene materials. *Small* **2011,** *7* (22), 3186-92.
21. Lin, S. Y.; Zhang, T. Y.; Lu, Q.; Wang, D. Y.; Yang, Y.; Wu, X. M.; Ren, T. L., High-performance graphene-based flexible heater for wearable applications. *Rsc Adv* **2017,** *7* (43), 27001-27006.
22. Kang, J.; Jang, Y.; Kim, Y.; Cho, S. H.; Suhr, J.; Hong, B. H.; Choi, J. B.; Byun, D., An Ag-grid/graphene hybrid structure for large-scale, transparent, flexible heaters. *Nanoscale* **2015,** *7* (15), 6567-73.
23. Deokar, G.; Avila, J.; Razado-Colambo, I.; Codron, J. L.; Boyaval, C.; Galopin, E.; Asensio, M. C.; Vignaud, D., Towards high quality CVD graphene growth and transfer. *Carbon* **2015,** *89*, 82-92.
24. Zhang, T. Y.; Zhao, H. M.; Wang, D. Y.; Wang, Q.; Pang, Y.; Deng, N. Q.; Cao, H. W.; Yang, Y.; Ren, T. L., A super flexible and custom-shaped graphene heater. *Nanoscale* **2017,** *9* (38), 14357-14363.
25. Romero, F. J.; Rivadeneyra, A.; Ortiz-Gomez, I.; Salinas, A.; Godoy, A.; Morales, D. P.; Rodriguez, N., Inexpensive Graphene Oxide Heaters Lithographed by Laser. *Nanomaterials-Basel* **2019,** *9* (9).
26. Alazmi, A.; Rasul, S.; Patole, S. P.; Costa, P. M. F. J., Comparative study of synthesis and reduction methods for graphene oxide. *Polyhedron* **2016,** *116*, 153-161.
27. Spruit, R. G.; van Omme, J. T.; Ghatkesar, M. K.; Garza, H. H. P., A Review on Development and Optimization of Microheaters for High-Temperature In Situ Studies. *J Microelectromech S* **2017,** *26* (6), 1165-1182.
28. Deokar, G.; Genovese, A.; Costa, P., Fast, wafer-scale growth of a nanometer-thick graphite film on Ni foil and its structural analysis. *Nanotechnology* **2020,** *31* (48), 485605.

29. Deokar, G.; Genovese, A.; Surya, S. G.; Long, C.; Salama, K. N.; Costa, P. M. F. J., Semi-transparent graphite films growth on Ni and their double-sided polymer-free transfer. *Sci Rep-Uk* **2020,** *10* (1).
30. <Kapton-10.1007_BF01106825.pdf>.
31. Comsol software. https://www.comsol.com/blogs/the-graphene-revolution-part-2/.
32. Zandi, S.; Saxena, P.; Gorji, N. E., Numerical simulation of heat distribution in RGO-contacted perovskite solar cells using COMSOL. *Sol Energy* **2020,** *197*, 105-110.
33. Fang, X. Y.; Yu, X. X.; Zheng, H. M.; Jin, H. B.; Wang, L.; Cao, M. S., Temperature- and thickness-dependent electrical conductivity of few-layer graphene and graphene nanosheets. *Phys Lett A* **2015,** *379* (37), 2245-2251.
34. Subrina, S.; Kotchetkov, D.; Balandin, A. A., Heat Removal in Silicon-on-Insulator Integrated Circuits With Graphene Lateral Heat Spreaders. *Ieee Electr Device L* **2009,** *30* (12), 1281-1283.
35. Mahlmeister, N. H.; Lawton, L. M.; Luxmoore, I. J.; Nash, G. R., Modulation characteristics of graphene-based thermal emitters. *Applied Physics Express* **2016,** *9* (1).
36. Wang, Y. Y.; Zhang, X.; Ding, X.; Li, Y.; Wu, B.; Zhang, P.; Zeng, X. L.; Zhang, Q.; Du, Y. H.; Gong, Y.; Zheng, K.; Tian, X. Y., Stitching Graphene Sheets with Graphitic Carbon Nitride: Constructing a Highly Thermally Conductive rGO/g-C3N4 Film with Excellent Heating Capability. *Acs Appl Mater Inter* **2021,** *13* (5), 6699-6709.
37. Luo, X. W.; Robin, J. C.; Yu, S. Y., Effect of temperature on graphite oxidation behavior. *Nucl Eng Des* **2004,** *227* (3), 273-280.
38. Pierson, H. O., *Handbook of carbon, graphite, diamond, and fullerenes: properties, processing, and applications*. 1st Edition ed.; New Jersey, 1994.
39. Batra, N. M.; Syed, A.; Costa, P. M. F. J., Current-induced restructuring in bent silver nanowires. *Nanoscale* **2019,** *11* (8), 3606-3618.
40. Kim, Y. R.; Jung, J. H.; Yong, S. M.; Hong, J. W.; Lee, S. J.; Park, J. W., Design of patterned fluorine-doped tin oxide for radome de-icing heater. *J Phys D Appl Phys* **2021,** *54* (10).
41. Zhang, Y.; Liu, H.; Tan, L. W.; Zhang, Y.; Jeppson, K.; Wei, B.; Liu, J. H., Properties of Undoped Few-Layer Graphene-Based Transparent Heaters. *Materials* **2020,** *13* (1).
42. Wang, X. D.; Guo, W.; Zhu, Y.; Liang, X. K.; Wang, F. D.; Peng, P., Electrical and Mechanical Properties of Ink Printed Composite Electrodes on Plastic Substrates. *Appl Sci-Basel* **2018,** *8* (11).
43. Kang, T. J.; Kim, T.; Seo, S. M.; Park, Y. J.; Kim, Y. H., Thickness-dependent thermal resistance of a transparent glass heater with a single-walled carbon nanotube coating. *Carbon* **2011,** *49* (4), 1087-1093.
44. Garcia, N.; Esquinazi, P.; Barzola-Quiquia, J.; Dusari, S., Evidence for semiconducting behavior with a narrow band gap of Bernal graphite. *New J Phys* **2012,** *14*.
45. Deng, S. K.; Berry, V., Wrinkled, rippled and crumpled graphene: an overview of formation mechanism, electronic properties, and applications. *Materials Today* **2016,** *19* (4), 197-212.
46. Grosse, K. L.; Bae, M. H.; Lian, F. F.; Pop, E.; King, W. P., Nanoscale Joule heating, Peltier cooling and current crowding at graphene-metal contacts. *Nat Nanotechnol* **2011,** *6* (5), 287-290.
47. Luo, F.; Fan, Y. S.; Peng, G.; Xu, S. G.; Yang, Y. P.; Yuan, K.; Liu, J. X.; Ma, W.; Xu, W.; Zhu, Z. H.; Zhang, X. A.; Mishchenko, A.; Ye, Y.; Huang, H.; Han, Z.; Ren, W. C.; Novoselov, K.

S.; Zhu, M. J.; Qin, S. Q., Graphene Thermal Emitter with Enhanced Joule Heating and Localized Light Emission in Air. *Acs Photonics* **2019,** *6* (8), 2117-2125.
48. Tokunaga, T.; Tranchant, L.; Takama, N.; Volz, S.; Kim, B., Experimental Study of Heat Transfer in Micro Glass Tubes Mediated by Surface Phonon Polaritons. *6th European Thermal Sciences Conference (Eurotherm 2012)* **2012,** *395*.
49. Giubileo, F.; Di Bartolomeo, A., The role of contact resistance in graphene field-effect devices. *Prog Surf Sci* **2017,** *92* (3), 143-175.
50. Deokar, G.; Vancso, P.; Arenal, R.; Ravaux, F.; Casanova-Chafer, J.; Llobet, E.; Makarova, A.; Vyalikh, D.; Struzzi, C.; Lambin, P.; Jouiad, M.; Colomer, J. F., MoS2-Carbon Nanotube Hybrid Material Growth and Gas Sensing. *Adv Mater Interfaces* **2017,** *4* (24).
51. Wu, J. B.; Cao, W. B.; Wen, W. J.; Chang, D. C.; Sheng, P., Polydimethylsiloxane microfluidic chip with integrated microheater and thermal sensor. *Biomicrofluidics* **2009,** *3* (1).
52. Sharma, B.; Kim, J. S., MEMS based highly sensitive dual FET gas sensor using graphene decorated Pd-Ag alloy nanoparticles for H-2 detection. *Sci Rep-Uk* **2018,** *8*.
53. Hoshino, S.; Yoshida, M.; Uemura, S.; Kodzasa, T.; Takada, N.; Kamata, T.; Yase, K., Influence of moisture on device characteristics of polythiophene-based field-effect transistors. *J Appl Phys* **2004,** *95* (9), 5088-5093.
54. Schedin, F.; Geim, A. K.; Morozov, S. V.; Hill, E. W.; Blake, P.; Katsnelson, M. I.; Novoselov, K. S., Detection of individual gas molecules adsorbed on graphene. *Nat Mater* **2007,** *6* (9), 652-655.